The Interictal Suppression Hypothesis in Focal Epilepsy: Electrographic and Structural Evaluation

Graham W. Johnson,[1,2,3] Derek J. Doss,[1,2,3] Victoria L. Morgan,[1,2,3,4,6,7] Danika L. Paulo,[4] Leon Y. Cai,[1,2,3] Jared S. Shless,[2,3,4] Aarushi S. Negi,[8] Abhijeet Gummadavelli,[4] Hakmook Kang,[9] Shilpa B. Reddy, [10] Robert P. Naftel,[4] Sarah K. Bick,[4] Shawniqua Williams Roberson,[6] Benoit M. Dawant,[1,2,3,4,5,7] Mark T. Wallace,[11,12,13,14] Dario J. Englot[1,2,3,4,5,7]

Author affiliations:

1 Vanderbilt University Department of Biomedical Engineering - Nashville, Tennessee, 37235 USA
2 Vanderbilt University Institute of Imaging Science (VUIIS) - Nashville, Tennessee, 37232 USA
3 Vanderbilt Institute for Surgery and Engineering (VISE) – Nashville, Tennessee, 37235 USA
4 Vanderbilt University Medical Center Department of Neurological Surgery - Nashville, Tennessee, 37232 USA
5 Vanderbilt University Department of Electrical Engineering and Computer Science - Nashville, Tennessee, 37235 USA
6 Vanderbilt University Medical Center Department of Neurology - Nashville, Tennessee, 37232 USA
7 Vanderbilt University Medical Center Department of Radiological Sciences - Nashville, Tennessee, 37232 USA
8 Vanderbilt University Department of Neuroscience - Nashville, Tennessee, 37232 USA
9 Vanderbilt University Department of Biostatistics - Nashville, Tennessee, 37232 USA
10 Vanderbilt Children's Hospital Department of Pediatrics - Nashville, Tennessee, 37232 USA
11 Vanderbilt University Department of Hearing and Speech Sciences - Nashville, Tennessee, 37232 USA
12 Vanderbilt University Department of Psychology - Nashville, Tennessee, 37232 USA
13 Vanderbilt University Department of Psychiatry and Behavioral Sciences - Nashville, Tennessee, 37232 USA
14 Vanderbilt University Department of Pharmacology - Nashville, Tennessee, 37232 USA

Correspondence to: Graham W. Johnson
Vanderbilt University
1500 21st Avenue South, VAV 4340
Nashville, Tennessee 37212
grahamwjohnson@gmail.com

Running title: Interictal suppression in focal epilepsy

Keywords: Epilepsy, connectivity, excitation suppression, EEG, diffusion imaging

Abbreviations: CRAVE CRAnial Vault Explorer, DRE drug-resistant epilepsy, DWI diffusion-weighted imaging, GABA gamma-aminobutyric acid, ImCoh imaginary coherence, ISH interictal suppression hypothesis, Non non-involved region, PDC partial directed coherence, PZ propagative zone, SEEG stereo-electroencephalography, SIFT2 spherical deconvolution filtering of tractograms, SOZ seizure onset zone, SPES single-pulse electrical stimulation, SVM support vector machine, SWiNDL Subsampling Whole-brain tractography with intracranial EEG Near-field Dynamic Localization, VUMC Vanderbilt University Medical Center.

Abstract

Why are people with focal epilepsy not continuously having seizures? Previous neuronal signaling work has implicated gamma-aminobutyric acid balance as integral to seizure generation and termination, but is a high-level distributed brain network involved in suppressing seizures? Recent intracranial electrographic evidence has suggested that seizure onset zones have increased inward connectivity which could be associated with interictal suppression of seizure activity. Accordingly, we hypothesize that seizure onset zones are actively suppressed by the rest of the brain network during interictal states.

Full testing of this hypothesis would require collaboration across multiple domains of neuroscience, including molecular, cellular, and brain network investigations. We focused on partially testing this hypothesis at the electrographic network level within 81 individuals with drug resistant focal epilepsy undergoing presurgical evaluation. We utilized intracranial electrographic resting-state and neurostimulation recordings to evaluate the network connectivity of seizure onset, early propagation, and non-involved regions. We then utilized diffusion imaging to acquire estimates of white matter connectivity to evaluate structure-function coupling effects on connectivity findings. Finally, using our observations, we generated a resting-state classification model to assist clinicians in detecting seizure onset and propagative zones without the need for multiple ictal recordings.

Our findings indicate that seizure onset and propagative zones demonstrate markedly increased inward connectivity and decreased outward connectivity using both resting-state (one-way ANOVA, p-value=3.13e-13) and neurostimulation analyses to evaluate evoked responses (one-way ANOVA, p-value=2.5e-3). When controlling for the distance between regions, the difference between inward and outward connectivity remained stable up to 80 mm between brain connections (two-way repeated measures ANOVA, group effect p-value of 2.6e-12). Structure-function coupling analyses revealed that seizure onset zones exhibit abnormally enhanced coupling (hypercoupling) of surrounding regions compared to presumably healthy tissue (two-way repeated measures ANOVA, interaction effect p-value of 9.76e-21). Using these observations, our support vector classification models achieved a maximum held-out testing set accuracy of 92.0±2.2% to classify early propagative and seizure onset zones.

These results suggest that seizure onset zones are actively segregated and suppressed by a widespread brain network. Furthermore, this electrographically observed functional suppression is disproportionate to any observed structural connectivity alterations of the seizure onset zones. These findings have implications for the identification of seizure onset zones using only brief electrographic recordings to reduce patient morbidity and augment the presurgical

evaluation of drug resistant epilepsy. Further testing of the interictal suppression hypothesis can provide insight into potential new resective, ablative, and neuromodulation approaches to improve surgical success rates in those suffering from drug resistant focal epilepsy.

Introduction

Drug resistant focal epilepsy (DRE) accounts for 30-40% of the estimated 50 million cases of epilepsy worldwide.[1, 2] If medication fails to control seizures, patients may elect to pursue surgical treatments including resection,[3, 4] ablation,[5, 6] or neurostimulation.[7, 8] Traditional presurgical evaluation includes identification of seizure-onset zones (SOZs) using seizure semiology, non-invasive neuroimaging and scalp EEG.[9] SOZs are defined as observed sites of ictal onset and are candidates for an electro-clinically defined "epileptogenic zone" that could theoretically be removed to render the patient seizure-free.[10] If these techniques fail to accurately localize SOZs, then invasive monitoring with stereotactic-EEG (SEEG) can be pursued.[11] To properly localize SOZs with SEEG, the patient must remain in the hospital for days to weeks to record many seizures (ictal events).[12, 13] To reduce the morbidity of long intracranial recordings, brief resting-state (interictal) SEEG analysis has shown promise in identifying SOZs.[14-20]

Resting-state SEEG studies often utilize the conceptual framework of epilepsy as a disorder of interconnected brain nodes (i.e. a network).[21-26] Specifically, recent work has shown that SOZs exhibit increased *inward* interictal connectivity from other nodes of the brain.[20, 27] This work has led us to propose the Interictal Suppression Hypothesis (ISH), which posits that the SOZ is tonically suppressed by other areas of the brain during the resting state to prevent seizure initiation (**Figure 1**). The premise of this hypothesis is intuitively based on the clinical observation that people with DRE are not continuously having seizures, so perhaps there is an interictal, widespread functional organization of the brain that is actively suppressing epileptiform activity. Further, neurophysiological evidence for this hypothesis has been demonstrated in animal models showing GABA (γ-aminobutyric acid) mediated receptor tonic interictal inhibition of SOZs.[28, 29] A complete testing of the ISH requires collaboration across many domains of neuroscience, including molecular, cellular, and brain network investigations utilizing both animal models and human data. In humans specifically, we can partially test the ISH by using SEEG electrodes to investigate the connectivity of the epileptic network. SEEG signal observations are electrical phenomena of underlying physiological activity which

provide direct sampling of brain tissue, offering insight into the high-level functional organization of the brain in humans with DRE.

Beyond resting-state recordings, SEEG electrodes can also be used to electrically stimulate the brain. Specifically, single-pulse electrical stimulation (SPES) can be used to simultaneously stimulate one region and record the post-stimulation EEG signal (evoked response) at all other implanted regions.[30-34] SPES provides another paradigm to test the ISH. Importantly, not only can directionality be inferred from SPES, but relative elevation or attenuation of oscillatory activity can also be quantified to gain insight into the relative excitatory and inhibitory nature of functional connections. Finally, the spatial and anatomical characteristics of the network (i.e. structural connectivity) have been shown to impact the resting-state and stimulation-derived network characteristics. Specifically, past work has suggest that short-range connection drive increased SOZ connectivity,[19] and diffusion-weighted imaging (DWI) derived structural connectivity helps explain the network's response to SPES.[35, 36] Using these techniques, we can evaluate the effects of distance and structural connectivity to further characterize the functional epileptic network.

Overall, this work aims to partially test the ISH at the brain network level using resting-state and stimulation-based electrophysiology, controlling for spatial and anatomical variability using DWI. Better characterization of SOZs using only interictal data may reduce patient morbidity by reducing reliance on ictal recordings and provide insight into the underlying biophysical pathophysiology of the epileptic network.

Materials and methods

Participants & Seizure Network Designations

We included 81 patients with DRE undergoing SEEG presurgical evaluation at Vanderbilt University Medical Center (VUMC). Important demographic and clinical variables are outlined in **Table 1.** This study was approved by Vanderbilt's Institutional Review Board and all patients provided informed consent. The diagnosis of DRE and decision to pursue SEEG were determined by VUMC's standard multidisciplinary process, including epileptologists, neurosurgeons, and neuropsychologists. This process included analysis of patient history, seizure semiology, video EEG, MRI, positron emission tomography, memory/language localization by functional MRI or Wada, and neuropsychological testing. Electrode (Ad-Tech,

Oak Creek, WI; or PMT Cooperation, Chanhassen, MN) trajectories were planned by treating physicians according to standard clinical care at VUMC using CRAnialVault Explorer (CRAVE; Vanderbilt University, Nashville, Tennessee).[37] Each patient had an average of 85.4 ± 26.7 (mean ± STD) SEEG contacts implanted in gray matter.

To assign seizure network designations to the SEEG contacts, the treating epileptologist reviewed all electroclinical ictal events during the SEEG monitoring. Seizure onset zones (SOZs) were defined as SEEG contact(s) with the first electrographic epileptiform changes observed for a clinically significant ictal event. Early propagation zones (PZs) were defined as SEEG contacts with electrographic epileptiform activity spread within 10 seconds of ictal onset. Finally, non-involved (Non) SEEG contacts were defined as belonging to neither SOZ or PZ designations.[19, 20] Finally, to quantify response to surgical intervention we calculated the Engel Surgical Outcome Scale for subjects who received a resective or ablative surgery and had follow-up data at least one year following surgery.[38] Patients who received a neuromodulation treatment were excluded from surgical outcome analyses.

Resting-state SEEG Connectivity

We calculated undirected and directed SEEG resting-state connectivity for all 81 subjects as outlined in our previous works.[19, 20] Briefly, we collected 20-minutes of resting-state data on SEEG post-implantation day one or two with the subject lying flat with their eyes closed trying not to fall asleep. We then filtered the data with a 1-59, 61-80 Hz bandpass Butterworth filter using Matlab's filtfilt function (MathWorks inc., Natick, MA, USA) to remove direct current offset and power line interference. The signals were referenced using a bipolar montage. For simplicity, each bipolar pair referenced signal will henceforth be referred to as a 'node', and the connectivity between two nodes will be referred to as an 'edge'. To reduce potential segmentation bias, we did not use a brain atlas for any portion of these analyses.[39] Avoiding potentially arbitrary region segmentations increases the generalizability of these analytical approaches and improves biological interpretation by only accounting for tissue that is directly sampled by SEEG. We then segmented the 20-minute resting-state epoch into 10 two-minute epochs. All metric calculations described below were averaged across these 10 two-minute epochs.

To assess undirected resting-state SEEG connectivity, we calculated imaginary coherence (ImCoh) for all edges.[19] For directed connectivity analysis, we calculated partial directed

coherence (PDC) for all edges.[20] A node's undirected connectivity was defined as the average ImCoh value of that node's edges with respect to all other nodes (i.e. 'strength' of the node). A node's outward connectivity was defined as the average outward PDC of edges with respect to all other nodes. Correspondingly, a node's inward connectivity was defined as the average inward PDC of edges from all other nodes. To quantify the overall direction of a node's connectivity, reciprocal connectivity was calculated as the difference between each node's inward and outward connectivity. All connectivity was analyzed in the theta [4-7 Hz], alpha [8-12 Hz], beta [12-30 Hz], and gamma [31-80 Hz] oscillatory bands.

Additionally, to evaluate the effect of distance on connectivity measurements, we calculated the Euclidean distance between all nodes (centroid of the bipolar pair) using CRAVE software. We then re-calculated all functional connectivity measurements with Euclidean edge distance thresholds of 5-20, 20-35, 35-50, 50-65, and 65-80 mm. These distance thresholds were chosen to include a roughly equal number of SEEG nodes across a wide range of Euclidean distances for the entire subject cohort. In this manner, we were able to observe the effect of distance between the SEEG nodes on the functional connectivity measurements.

Single-Pulse Electrical Stimulation (SPES) Connectivity

To further test the ISH, we collected neurostimulation data from the most recently enrolled subset of 23 patients in the cohort. Specifically, we conducted SPES with every SEEG node in gray matter for each patient, resulting in 60.0 ± 10.7 (mean ± STD) nodes stimulated per patient. We used 10-second trains of 1 Hz, 300 μs, biphasic pulses at 3.0 mA with a recording sampling rate of 512 Hz. We filtered raw SEEG data using Matlab's filtfilt function with Butterworth filters with passbands of 1-59 and 61-80 Hz. We then parsed the data into epochs of 5-305 ms following each stimulation pulse. This post-stimulation epoch has been previously outlined to capture the majority of SPES-induced electrographic changes.[31] The initial 5 ms epoch following stimulation and all nodes within 20 mm of stimulation were omitted to avoid stimulation artifact.[40]

We then created SPES-derived connectivity matrices by computing the power spectral density (PSD) for the frequency bands outlined in "Resting-State SEEG Connectivity". The PSD for each node was normalized to that node's pre-stimulation baseline value. The outward connectivity for a given node was assigned as the PSD change from baseline within a given frequency range for all non-stimulated SEEG nodes when that node was stimulated.

Conversely, the inward connectivity for a given node was assigned as the PSD change from the pre-stimulation baseline in the frequency band of interest for that node when all other nodes had been stimulated separately. All PSD measurements were averaged across the 10 redundant stimulation pulses to increase the signal-to-noise ratio. We did not attempt to analyze any frequencies below 4 Hz due to the short sampling window post-stimulation.

Diffusion Imaging Collection & Preprocessing

We collected DWI data using high angular resolution diffusion imaging acquisition with 92 b-vector directions at a b-value of 1600 s/mm^2. We preprocessed the DWI data with a pipeline built around MRTrix3[41], FSL[42], and ANTs[43] software packages.[44] First, the diffusion data were denoised with the Marchenko-Pastur PCA method.[45-47] The images were then intensity-normalized to the first image and concatenated for further processing. No reverse phase encoded images were acquired, but corresponding T1 images of the subjects were available. Thus, a T1 image was used to generate a synthetic susceptibility-corrected b0 volume using SYNB0-DISCO, a deep learning framework by Schilling et al.[48] This synthetic b0 image was used in conjunction with FSL's topup to correct for susceptibility-induced artifacts in the diffusion data. FSL's eddy algorithm was then used to correct motion artifacts and eddy currents and to remove outlier slices.[49-52]

Patient Specific SEEG-Based Structural Connectivity: The SWiNDL Technique

Next, we sought to evaluate the structure-function coupling between brain regions sampled by SEEG. To accurately quantify the structural connectivity between SEEG electrodes, we implemented a novel technique termed "Subsampling Whole-Brain Tractography with iEEG Near-Field Dynamic Localization" (SWiNDL). We developed this technique to obtain a patent-specific SEEG contact-to-contact structural connectome by utilizing the group analysis advantages of anatomically constrained whole-brain tractography and spherical deconvolution filtering of tractograms (SIFT2).[53]

First, we performed whole-brain tractography using MRtrix3 with SIFT2 weighting to generate ten million streamlines.[41, 53] Briefly this included brain extraction from the T1 image[54], bias field correction,[55] and registration to DWI[56]. The T1 image was then be used to create 5-

tissue type (5TT)[57-59] segmentations. Spherical deconvolution was performed on the preprocessed DWI to get direct fiber orientation density function for every voxel.[60, 61] We then performed probabilistic tractography[62] utilizing the 5TT volume to perform anatomically constrained tractography[63] with dynamic seeding.[49] The resulting tractogram was then corrected using spherical-deconvolution informed filtering of tractograms (SIFT2) for improved biological accuracy of white-matter representation.[53, 64]

We then localized each patient's SEEG electrodes using CRAVE. We assigned a three-dimensional Gaussian probability distribution around each SEEG contact to model the volume of tissue electrically sampled by that electrode – we used a 95% attenuation of the probability at 12 mm based off previous electrophysiological work characterizing the spatial dynamics of local field potentials.[65] For the connection between each pair of SEEG contacts (i.e. an edge), we then took the raw tractogram of 10 million streamlines and assigned dynamic weights [0-1] to each streamline based on the location of the endpoints relative to the SEEG contacts. For example, a streamline would be highly sampled by the SWiNDL algorithm with a weight close to 1.0 if each endpoint were near the center of a contact. Whereas if one or both endpoints were far from the two SEEG contacts of interest, then that streamline would be assigned a weight close to 0.0 based off the minimum Gaussian distribution value of the two contacts. The weighted sum of the 10 million streamlines for each bivariate pair of contacts is summed to achieve the structural connectivity for that edge. SWiNDL allows for patient-specific SEEG contact-level connectomes that are dynamically weighted to the proximity of streamlines to the contacts and does not rely on inconsistent probabilistic tractography seeding between patients.

Using the SWiNDL structural connectivity, we calculated the average connectivity for SOZs, PZs, and non-involved regions across a subset of 26 subjects that had available diffusion imaging. Finally, we evaluated the structure-function coupling by calculating the ratio of structural/functional connectivity for each SEEG edge within a patient. Well-coupled structural and functional connections are expected to have a relative ratio of unity. Thus, we termed any connections that had disproportionality high functional connectivity compared to average or low structural connectivity as "hypercoupled".

SEEG Node Classification Model

Using the functional and structural connectivity metrics outlined above, we sought to test the efficacy of a support vector machine (SVM) classification of individual SEEG nodes (i.e.

bipolar channel pairs) as SOZ, PZ or non-involved. For all SVM model development and evaluation we utilized a 5-fold nested cross-validation scheme (**Figure 7A**) that utilizes a completely held out test set for each fold of model training and validation. This way, we can repeatedly test a model's generalizability while minimizing overfitting the training data. All fold splits were conducted at the patient level.

First, we developed a model to classify each SEEG node as SOZ, PZ, or non-involved using only the resting-state functional connectivity metrics of ImCoh and PDC (6928 SEEG nodes for 81 subjects). Next, we sought to evaluate if the model improved with the addition of patient-specific structural connectivity metrics obtained from SWiNDL evaluation of DWI (2051 SEEG nodes from 26 subjects). Finally, we trained a model using only functional data from subjects who received resective or ablative therapy and achieved Engel I (free of disabling seizures) outcomes at least one year after surgery (1431 SEEG nodes from 19 subjects), and then evaluated the model on subjects who received resective or ablative therapy with Engel II-IV (not seizure free) surgical outcomes (1265 SEEG nodes from 15 subjects).

Data availability

Data may be made available upon reasonable request.

Results

SOZs and PZs Exhibit Evidence of Network Suppression at Rest

Resting-state SEEG analysis with 81 subjects revealed that SOZs and PZs exhibit significantly increased undirected connectivity compared to non-involved regions. These results were consistent across all frequency bands. The alpha band results are depicted in **Figure 2A** (one-way ANOVA, p-value=2.13e-3 with post-hoc multiple pairwise t-test comparisons depicted in figure). For the directed analysis, SOZs and PZs demonstrated markedly elevated inward connectivity and lower outward connectivity compared to non-involved regions. More specifically, the mean PZ inward and outward connectivity was significantly intermediate to the SOZ and non-involved mean (**Figure 2B-C**, one-way ANOVA, p-values=1.75e-12, post-hoc pairwise t-test p-value 4.95e-10 for inward and outward respectively). The reciprocal connectivity (inward – outward) exhibited an increased significance with a one-way ANOVA p-value of 3.13e-13 (**Figure 2D**). As with undirected connectivity, the directed results were

consistent across all frequency bands (one-way ANOVA, p-value<1e-10 for all bands). These findings suggest that high-level functional organization of the epileptic network, as observed on resting-state SEEG, exhibits a very high inward flow of information to SOZs and PZs characterized by elevated inward connectivity and lower outward connectivity.

Low Frequency Power is Attenuated in SOZs When the Network is Stimulated

When conducting SPES on non-SOZ SEEG contacts, we observed that the SOZ power was markedly attenuated compared to baseline and significantly attenuated compared to non-involved regions in the lowest frequency band measured (theta, 4-7 Hz) for the 23 patients consented for neurostimulation (**Figure 3A**, SOZ single-population t-test, p-value=2.28e-4, one-way ANOVA, p-value=2.50e-3, post-hoc pairwise t-test comparison SOZ-Non, p-value=1.80e-3). The SOZ and PZ power was not significantly altered in the alpha band [8-12 Hz] (**Figure 3B**). The SOZ and PZ power was elevated compared to baseline in both beta [13-30 Hz] and gamma bands [31-80 Hz], but post-hoc multiple comparisons revealed that the SOZ elevation in power was only significantly different from non-involved regions in the beta band and only from PZs in the gamma band (**Figure 3C-D**, beta: SOZ single-population t-test p-value=9.00e-3, one-way ANOVA p-value=2.98e-2, post-hoc pairwise t-test comparison SOZ-Non p-value=2.24e-2; gamma: SOZ single-population t-test p-value=6.70e-3, one-way ANOVA p-value=1.11e-2, post-hoc pairwise t-test comparison SOZ-PZ p-value=1.33e-2). These results indicate that low-frequency power is markedly attenuated in SOZs, but not PZs or non-involved regions when other nodes of the network are stimulated.

Inward vs. Outward Connectivity Remains Constant Over Long Distances

When evaluating the effects of distance on functional connectivity on all 81 patients in the cohort, we observed that both undirected and directed connectivity dropped significantly as Euclidean edge length increased (**Figure 4A-C**, two-way repeated measures ANOVA distance effect p-value<1e-10 for undirected inward and outward connectivity). Furthermore, the SOZ, PZ and non-involved region undirected connectivity 95% confidence intervals of the mean overlapped significantly for edge distances greater than 20 mm. However, inward and outward

connectivity for SOZs, PZs and non-involved regions remained significantly different from each other over the span of Euclidean edge distances (two-way repeated measures ANOVA group effect p-value<1e-10 for inward and outward). Calculating the reciprocal connectivity over distance, we observed that the relationship between inward vs. outward connectivity remained mostly consistent over the span of distances as can be observed by the flattening of the trends in **Figure 4D** compared to prior plots (two-way repeated measures ANOVA group effect p-value=2.6e-12, interaction p-value=1.15e-6). These results indicate that the network's potential functional suppression of SOZs and PZs, as measured by increased inward connectivity and decreased outward connectivity, scales proportionally as distance increases – thus suggesting whole network involvement in SOZ and PZ activity regulation despite the apparent large contribution of only local regions.

SOZs Exhibit Local Structure-Function Hypercoupling

Using the SWiNDL technique on 26 patients with DWI available, we observed that SOZs and PZs demonstrated comparably increased structural connectivity compared to non-involved regions despite only SOZs exhibiting significantly increased reciprocal functional connectivity in this cohort (**Figure 5A**, Structural: one-way ANOVA p-value=5.18e-7, SOZ-PZ p-value=1.2e-3, SOZ-Non p-value=3.30e-7; Functional: one-way ANOVA p-value=2.92e-8, SOZ-Non p-value=7.88e-7, PZ-Non p-value=5.13e-7). This suggests that SOZs have enhanced functional suppression to PZs despite a comparable SEEG-specific structural connectivity.

We then observed that only the local (5-20 mm) structural connectivity of SOZ and PZs appears to be driving the observed increase in structural connectivity over non-involved regions due to the overlapping of 95% confidence intervals for all distance thresholds greater than 20 mm (**Figure 5B**). However, the structure-function hypercoupling of SOZs was significantly stronger extending out to 35 mm compared to non-involved regions, with PZs exhibiting an intermediate local (5-20 mm) structure-function hypercoupling (**Figure 5C**, two-way repeated measures ANOVA group effect p-value=7.27e-4, distance effect p-value=8.63e-19, interaction p-value=9.76e-21). These results indicate that SOZs exhibit an inherently increased resting-state structure-function suppressive hypercoupling over short to medium range distances despite a comparable structural connectivity to that of PZs.

PZ Connectivity Differs Based on Surgical Outcome

When re-evaluating resting-state SEEG functional connectivity over distance in subjects with Engel I vs. Engel II-IV surgical outcomes, we observed that PZs exhibited the largest identifiable difference in connectivity profiles. Specifically, PZs exhibit an intermediate connectivity profile to that of SOZs and non-involved regions in subjects with Engel I outcomes (**Figure 6**, two-way repeated measures ANOVA group effect p-value = 1.16e-2, distance effect -value=1.26e-2, interaction p-value=5.15e-2). Conversely, PZ 95% confidence intervals become indistinguishable from non-involved regions and significantly different from SOZs for subjects with Engel II-IV outcomes (**Figure 6B**, two-way repeated measures ANOVA group effect p-value=1.73e-4, distance effect p-value=7.83e-1, interaction p-value=3.01e-3). Finally, the mean variance of SOZ vs. PZ reciprocal connectivity was 0.414 for Engel I and 0.280 for Engel II-IV (two-sample t-test p=0.394), indicating that PZ connectivity in Engel II-IV subjects was not only lower, but also more consistently resembled non-involved region connectivity compared to Engel I subjects. These results could indicate a fundamental difference of PZ connectivity in subjects with Engel II-IV surgical outcome or could reflect different SEEG sampling and subsequently different ictal event interpretation in these subjects.

A Structure-Function Coupling Model Most Accurately Classifies SEEG Nodes as SOZ, PZ, or Non-Involved Region.

Using a nested cross validation model (**Figure 7A**), we first trained an SVM with only the resting-state SEEG functional connectivity data summarized in **Figure 2** to classify individual SEEG nodes as residing in an SOZ, PZ or non-involved region (**Figure 7B**). The model achieved an overall accuracy of 84.4% (±2.1% standard deviation, SD) and individual true positive rates of 92.0±6.9% for SOZs, 81.6±5.4% for PZs and 53.0±1.8% for non-involved regions. Incorporating SWiNDL structural connectivity derived from DWI data into the model raised the test set overall accuracy to 92.0±2.2% and the individual true positive rates to 92.5±7.2% for SOZs, 93.0±5.3% for PZs and 71.2±2.0% for non-involved regions (**Figure 7C**).

We then sought to test the accuracy of a functional connectivity model only trained on Engel I outcome subjects (**Figure 7D**). For this model, the test set overall model accuracy increased compared to the accuracy for the entire cohort to 89.5±2.8%, with true positive rate

increasing for PZ and non-involved regions and remaining unchanged for SOZs. Next, when using the Engel I model on Engel II-IV subjects, the accuracies dropped to 67.1±0.4%. Overall, these findings suggest that a model trained on readily available resting-state SEEG data can accurately classify SOZs, PZs, and non-involved regions, but accuracy increases if DWI data are available. Furthermore, the large drop in accuracy when using the Engel I model on Engel II-IV subjects could suggest that Engel II-IV subjects have a fundamentally different connectivity profile to that of subjects who achieved Engel I outcomes. Alternatively, this drop in model performance could be attributed to clinically-defined SOZ (and thus potential EZs) being more likely to be inaccurate in patients with Engel II-IV outcomes.

Discussion

The concept of excitation and inhibition in epilepsy has been investigated for decades.[29, 66-68] Specifically, at the cellular level, GABA signaling is thought to play a pivotal role in seizure initiation and termination when investigated *in vitro*, *ex vivo*, and with optogenetics.[69-71] When abstracted to electrographic networks, the concept of inhibition and excitation has been explored as it relates to inward and outward connectivity of epileptogenic zones. Recent evidence has suggested that epileptogenic zones have increased inward connectivity which could relate to interictal suppression of epileptiform activity.[19, 20, 72-78] Whereas other works have focused on observations of increased outward connectivity from SOZs to the rest of the network.[31, 79, 80] In response to the existing variety of observations and interpretations of functional connectivity in the epileptic network, this work sought to partially test the specific hypothesis of interictal suppression of SOZs (the ISH) at the electrographic network level by characterizing the direction and relative elevation or attenuation of neural activity.

Properly testing the ISH with only resting-state SEEG connectivity is challenging due to the difficulty of interpreting whether resting-state functional connectivity is excitatory, inhibitory, or neutral. For example, increased inward connectivity could be interpreted with known directed connectivity motifs,[81] but it will not directly indicate if this increase in inward connectivity correlates to any region being suppressed or excited. Thus, we conducted SPES to 1) provide additional insight into the directionality of network connectivity with another paradigm, and 2) quantify elevation or attenuation of frequency band power by measuring the change in relative band power from pre-stimulation baseline. Using SPES, we can gain insight into the potential excitatory and inhibitory nature of the network connectivity. However, it is

important to consider that SPES itself may be altering the network dynamics away from the resting state. Thus, interpretation of resting-state SEEG and SPES findings must be carefully integrated.

Further complicating this discussion, one cannot assume that attenuation in a certain frequency band power aligns with inhibition. As an example, there is a large body of evidence that an *increase* in beta power correlates to *inhibition* of motor circuits, particularly in Parkinson's disease.[82, 83] For the sake of clarity, we will use the term 'elevation' to refer to an increase in signal band power, and 'attenuation' to refer to a decrease. We will reserve the terms 'excitation' and 'inhibition/suppression' for the concept of how a modification in neural activity relates to a change in a clinically observable behavior of interest (e.g. seizure vs. no seizure). Furthermore, we use the term "seizure onset zone" to indicate an area of first observed electrographic epileptiform changes. We reserve the use of the term "epileptogenic zone" (i.e. "site of the beginning of the epileptic seizures and of their primary organization") for discussion of an electro-clinically defined region that must be resected to render the subject seizure free and typically contains a SOZ.[10] With these considerations and definitions in mind, we will discuss our interpretation of the pertinent findings in this work.

Does Imbalanced Reciprocal Connectivity Indicate Suppression?

In this study, we observed imbalanced reciprocal (inward – outward) connectivity of SOZs and PZs: Specifically, SOZs demonstrated a large increase in inward connectivity and a moderate decrease in outward connectivity in resting-state SEEG analyses. PZs exhibited a similar imbalance in reciprocal connectivity to SOZs, but to an intermediate extent. Important for interpretation, non-involved region reciprocal connectivity was approximately zero – i.e. regions not directly involved in seizure onset or early propagation have roughly equal inward and outward connectivity. This suggests that SOZs and PZs interact with the network differently than presumably healthy regions of the brain. One interpretation of this finding is that SOZs are actively isolated/segregated by other regions of the brain. It is possible that healthy regions are sending inhibitory signals to the SOZs and PZs (increased inward connectivity) and thus suppress their ability to communicate with the rest of the network and initiate seizures (decreased outward connectivity).

Further evidence for SOZ segregation was exhibited in the reciprocal connectivity elucidated with low-frequency stimulation. Using a power spectral density approach,[74, 84, 85] we intended to build on previous works that focused on whole-band power metrics like root mean square,[77, 79, 86] or metrics that rely on cortico-cortical evoked potential waveform morphology which can be difficult to interpret with depth electrodes.[75, 87-91] Overall, when presumably healthy regions were stimulated, the SOZ theta [4-8 Hz] relative band power was markedly decreased from pre-stimulation baseline. Conversely, SOZ beta [13-30 Hz] and gamma [31-80 Hz] relative band power increased when healthy regions were stimulated. Increased inward evoked gamma band power in SOZs is in alignment with previous low-frequency stimulation findings.[74] Notably, reciprocal evoked alpha band power was not altered across all region designations, and PZ relative band power was not significantly altered for any frequency band measured.

It is long known that theta spectral power accounts for a significantly larger portion of whole band power on EEG recordings compared to beta and gamma power.[92] Additionally, theta power is thought to be involved with long range integration of brain regions, whereas gamma power is considered important for local integration.[93-95] Thus, simultaneous attenuation of a high-power spectral band (theta), in parallel with excitation of a locally integrating frequency band (gamma), suggests that SOZ functional segregation is increased when non-involved regions are stimulated. Furthermore, gamma activity is thought to reflect GABA inhibitory interneuron activity.[96-98] Thus, increased inwardly activated gamma band power in SOZs could reflect a direct change in the GABA interneuron balance. Additionally important to consider is that gamma activity, in the form of low-voltage fast activity, is commonly observed on intracranial EEG immediately before ictal onset and increased baseline gamma power is thought to be a biomarker for the "ictal core".[99-101] Thus, it is possible that the observed SOZ increase in gamma power when non-SOZ nodes are stimulated is simply SOZs demonstrating an enhancement of an intrinsic pathologically distinct phenomenon and could actually be driving SOZs toward an ictal state. Finally, previous work has shown that post-stimulation SOZ decrease in low frequency power and increase in high-frequency power correlates to favorable surgical outcome.[102] Overall, the SPES findings provide corroborating evidence for an electrographic network-level increase in inward connectivity to the SOZ and provide insight into the frequency-specific behavior of SOZs during stimulation, but more work is needed to further test the ISH.

Reciprocal Connectivity is Edge Distance Invariant, but SOZs Exhibit Local Structure-Function Hypercoupling

We sought to investigate if findings of increased inward connectivity to SOZs were affected by Euclidean distance and/or estimates of anatomical white matter connectivity between SEEG contacts. Past work has demonstrated the importance of considering Euclidean edge distance when analyzing functional epileptogenic networks.[103] Specifically, it has been demonstrated that short-range structural connections drive the majority of aberrant SOZ connectivity and could dictate seizure spread.[19, 104, 105] This observation of rapid functional connectivity decay with increasing edge length was recapitulated in this work's undirected and directed resting-state findings. However, long range connections are thought to add diversity and complexity to brain networks and could be important contributors to widescale integration.[106] Concordantly, our finding that resting-state reciprocal connectivity is relatively constant across distance suggests that distant brain regions may still play an important role in SOZ excitation and inhibition.

Beyond simple Euclidean distance metrics, diffusion-derived structural connectivity characteristics can be used to investigate potential pathological SOZ connectivity.[107-113] We observed SOZs and PZs to have increased structural connectivity relative to non-involved regions, which is in alignment with past SEEG-informed diffusion imaging studies.[108] This increase could represent an intrinsic pathological biomarker of the epileptogenic network or could possibly be due to implantation bias increasing the density of SEEG contacts around suspected SOZs. Of more pertinent interest to testing the ISH, we investigated if structural connectivity variation could explain our observed differences in functional connectivity. The "coupling" between structure and function is the term commonly used when the strength of structural connections predicts the strength of functional connections.[114] Thus, a region exhibits strong structure-function coupling when the ratio of their relative functional and structural connections is unity. We use the term "hypercoupling" to refer to connections that exceed the functional connection strength expected from structural connectivity. We observed that SOZs demonstrate markedly increased local hypercoupling – i.e. the increased inward functional connectivity strength is disproportionally elevated above the average structure-function coupling by two standard deviations for edge connections within 5-20 mm. This suggests an abnormal functional reorganization around the SOZs disproportionate to any alterations in structural connectivity.

Proper PZ Identification May Help Prognosticate Surgical Outcome

A sub analysis with Engel I vs. Engel II-IV surgical resection outcomes demonstrated that PZ connectivity resembled non-involved region connectivity in Engel II-IV subjects. This could be due to an intrinsic difference in PZ connectivity between surgical responders and non-responders, a difference in SEEG implantation strategy between the patient groups that affects network observations, or a difference in ictal interpretation that affects node designation.[115-117] With this observation as motivation, we developed SVM models to classify SOZs, PZs, and non-involved regions. The models were able to classify SOZs with very high accuracy (range of 91.4-92.5% accuracy) but differed in ability to differentiate PZs from non-involved regions (range of 81.6-93.0% accuracy). Notably, our SVM model to classify individual SEEG bipolar pairs confused PZs and non-involved regions when the entire subject cohort was used in model generation and testing (31.9% false identification of PZs as non-involved regions). When restricted to Engel I subjects, the model improved classification between PZs and non-involved regions (21.1%), with subsequently very poor performance when this model was used to test Engel II-IV subjects. Of note, the best model was produced when diffusion-derived metrics were included, but these data are less commonly collected during presurgical workup. Overall, the models very accurately classified SOZs, but we encourage other groups to include PZ classification into model design because it may be an important factor for prognosticating surgical outcome.

Limitations

This work utilizes multiple analysis techniques to test the ISH but is limited by the ambiguity of network neuroscience interpretation and integration. Electrographic phenomena observed on SEEG and probabilistic tractography performed on diffusion imaging are removed from underlying neurophysiology and neuropathology. Thus, interpretation of functional and structural network connectivity findings must resist the proclivity toward self-justified and circular conclusions. Further complicating interpretation is the lack of control groups for these populations. SEEG control data does not exist, and we did not include neuroimaging controls. All scientific inferences and hypothesis testing were conducted on comparisons to regions presumably not involved in the genesis or early propagation of epileptiform activity. For

subjects with epilepsy, it could be reasonable to assume that the entire brain network is sick and thus intra-patient normalization to “healthy” regions could be an ill-posed analytical model. As more depth electrodes are being used for therapy in people with varying psychiatric and neurological disorders, large-scale data sharing to expand our understanding of baseline electrographic phenomena across a more diverse population could help address these issues.

Conclusions

In summary, using resting-state SEEG analyses and low-frequency stimulation, we observed electrographic evidence of interictal functional suppression of SOZs and PZs and thus supporting in the ISH. When controlling for distance and structural connectivity, we found that SOZs and PZs demonstrate consistent long-range relative reciprocal connectivity, but elevated local hypercoupling of functional connectivity that could indicate enhanced interictal suppression of SOZs. Finally, we have demonstrated that a clinically useful model can be generated using only SEEG data to classify SOZs, PZs, and non-involved regions. However, inclusion of DWI-derived structural connectivity can increase the model accuracy. Overall, we believe this work supports the hypothesis of interictal suppression of SOZs and could have practical implications to reduce the morbidity of the presurgical workup and aid clinical decision making for this devastating neurological disorder.

Acknowledgements

We would like to thank the patients for participating in this investigation.

Funding

This work was supported by the following funding sources: NINDS R00-NS097618-05, NINDS R01-NS112252-02, NINDS R01-NS075270, NINDS R01-NS110130, NINDS R01-NS108445, NINDS F31-NS106735, and NIH Training Grants: NIGMS T32-GM007347, NIBIB T32-EB021937, and NIBIB T32EB001628.

Competing interests

The authors report no competing interests.

Supplementary material

Supplementary material is available at *Brain* online.

References

1. Behr C, Goltzene MA, Kosmalski G, Hirsch E, Ryvlin P. Epidemiology of epilepsy. *Revue Neurologique*. 2016;172(1):27-36. doi:10.1016/j.neurol.2015.11.003
2. Engel J, Jr. What can we do for people with drug-resistant epilepsy? The 2016 Wartenberg Lecture. *Neurology*. Dec 06 2016;87(23):2483-2489. doi:10.1212/WNL.0000000000003407
3. Englot DJ, Chang EF. Rates and predictors of seizure freedom in resective epilepsy surgery: an update. *Neurosurgical review*. Jul 2014;37(3):389-404; discussion 404-5. doi:10.1007/s10143-014-0527-9
4. Engel J, Jr., McDermott MP, Wiebe S, et al. Early surgical therapy for drug-resistant temporal lobe epilepsy: a randomized trial. Multicenter Study Randomized Controlled Trial Research Support, N.I.H., Extramural. *Jama*. Mar 7 2012;307(9):922-30. doi:10.1001/jama.2012.220
5. Wu C, Jermakowicz WJ, Chakravorti S, et al. Effects of surgical targeting in laser interstitial thermal therapy for mesial temporal lobe epilepsy: A multicenter study of 234 patients. *Epilepsia*. Jun 2019;60(6):1171-1183. doi:10.1111/epi.15565
6. Wicks RT, Jermakowicz WJ, Jagid JR, et al. Laser Interstitial Thermal Therapy for Mesial Temporal Lobe Epilepsy. *Neurosurgery*. Dec 2016;79 Suppl 1:S83-S91. doi:10.1227/NEU.0000000000001439
7. Englot DJ, Birk H, Chang EF. Seizure outcomes in nonresective epilepsy surgery: an update. *Neurosurgical review*. May 21 2017;40(2):181-194. doi:10.1007/s10143-016-0725-8
8. Boon P, De Cock E, Mertens A, Trinka E. Neurostimulation for drug-resistant epilepsy: a systematic review of clinical evidence for efficacy, safety, contraindications and predictors for response. *Curr Opin Neurol*. Apr 2018;31(2):198-210. doi:10.1097/WCO.0000000000000534
9. Parvizi J, Kastner S. Promises and limitations of human intracranial electroencephalography. *Nat Neurosci*. Apr 2018;21(4):474-483. doi:10.1038/s41593-018-0108-2
10. Kahane P, Landré E, Minotti L, Francione S, Ryvlin P. The Bancaud and Talairach view on the epileptogenic zone: a working hypothesis. *Epileptic Disord* 2006;8(2):S16-26.
11. Khoo HM, Hall JA, Dubeau F, et al. Technical Aspects of SEEG and Its Interpretation in the Delineation of the Epileptogenic Zone. *Neurol Med Chir (Tokyo)*. Nov 6 2020;doi:10.2176/nmc.st.2020-0176
12. Rheims S, Ryvlin P. Patients' safety in the epilepsy monitoring unit: time for revising practices. *Current opinion in neurology*. 2014;27(2):213-218.
13. Karthick P, Tanaka H, Khoo HM, Gotman J. Could we have missed out the seizure onset: A study based on intracranial EEG. *Clinical Neurophysiology*. 2020;131(1):114-126.
14. Cimbalnik J, Klimes P, Sladky V, et al. Multi-feature localization of epileptic foci from interictal, intracranial EEG. *Clinical Neurophysiology*. 2019;130(10):1945-1953. doi:10.1016/j.clinph.2019.07.024
15. Taylor PN, Papasavvas CA, Owen TW, et al. Normative brain mapping of interictal intracranial EEG to localize epileptogenic tissue. *Brain*. 2022;doi:10.1093/brain/awab380
16. Weiss SA, Staba RJ, Sharan A, et al. Accuracy of high-frequency oscillations recorded intraoperatively for classification of epileptogenic regions. *Scientific Reports*. 2021;11(1)doi:10.1038/s41598-021-00894-3
17. Frauscher B. Localizing the epileptogenic zone. *Curr Opin Neurol*. Apr 2020;33(2):198-206. doi:10.1097/WCO.0000000000000790
18. Balaji SS, Parhi KK. Seizure Onset Zone Identification From iEEG: A Review. *IEEE Access*. 2022;10:62535-62547. doi:10.1109/access.2022.3182716
19. Goodale SE, González HFJ, Johnson GW, et al. Resting-State SEEG May Help Localize Epileptogenic Brain Regions. *Neurosurgery*. 2020;86(6):792-801. doi:10.1093/neuros/nyz351

20. Narasimhan S, Kundassery KB, Gupta K, et al. Seizure-onset regions demonstrate high inward directed connectivity during resting-state: An SEEG study in focal epilepsy. *Epilepsia*. 2020;61(11):2534-2544. doi:10.1111/epi.16686
21. Foit NA, Bernasconi A, Bernasconi N. Functional Networks in Epilepsy Presurgical Evaluation. *Neurosurg Clin N Am*. Jul 2020;31(3):395-405. doi:10.1016/j.nec.2020.03.004
22. Larivière S, Bernasconi A, Bernasconi N, Bernhardt BC. Connectome biomarkers of drug-resistant epilepsy. *Epilepsia*. 2021;62(1):6-24. doi:10.1111/epi.16753
23. Royer J, Bernhardt BC, Larivière S, et al. Epilepsy and brain network hubs. *Epilepsia*. 2022;doi:10.1111/epi.17171
24. Stacey W, Kramer M, Gunnarsdottir K, et al. Emerging roles of network analysis for epilepsy. *Epilepsy Res*. Jan 2020;159:106255. doi:10.1016/j.eplepsyres.2019.106255
25. Johnson GW, Doss DJ, Englot DJ. Network dysfunction in pre and postsurgical epilepsy: connectomics as a tool and not a destination. *Curr Opin Neurol*. Apr 1 2022;35(2):196-201. doi:10.1097/WCO.0000000000001008
26. Sinha N, Johnson GW, Davis KA, Englot DJ. Integrating Network Neuroscience Into Epilepsy Care: Progress, Barriers, and Next Steps. *Epilepsy Currents*. 2022:153575972211012. doi:10.1177/15357597221101271
27. Gunnarsdottir KM, Gonzalez-Martinez J, Wing S, Sarma SV. Sources and Sinks in Interictal iEEG Networks: An iEEG Marker of the Epileptogenic Zone. IEEE; 2021:
28. Pavlov I, Walker MC. Tonic GABA(A) receptor-mediated signalling in temporal lobe epilepsy. *Neuropharmacology*. Jun 2013;69:55-61. doi:10.1016/j.neuropharm.2012.04.003
29. Engel J. Excitation and Inhibition in Epilepsy. *Canadian Journal of Neurological Sciences / Journal Canadien des Sciences Neurologiques*. 1996;23(3):167-174. doi:10.1017/s0317167100038464
30. Valentin A, Anderson M, AlarcoÂn G, et al. Responses to single pulse electrical stimulation identify epileptogenesis in the human brain in vivo. *Brain*. 2002;125(8):1709-1718. doi:10.1093/brain/awf187
31. Matsumoto R, Kunieda T, Nair D. Single pulse electrical stimulation to probe functional and pathological connectivity in epilepsy. *Seizure*. 2017;44:27-36. doi:10.1016/j.seizure.2016.11.003
32. Flanagan D, Valentín A, García Seoane JJ, Alarcón G, Boyd SG. Single-pulse electrical stimulation helps to identify epileptogenic cortex in children. *Epilepsia*. 2009;50(7):1793-1803. doi:10.1111/j.1528-1167.2009.02056.x
33. Boido D, Kapetis D, Gnatkovsky V, et al. Stimulus-evoked potentials contribute to map the epileptogenic zone during stereo-EEG presurgical monitoring. *Human Brain Mapping*. 2014;35(9):4267-4281. doi:10.1002/hbm.22516
34. Kundu B, Davis TS, Philip B, et al. A systematic exploration of parameters affecting evoked intracranial potentials in patients with epilepsy. *Brain Stimulation*. 2020;13(5):1232-1244. doi:10.1016/j.brs.2020.06.002
35. Crocker B, Ostrowski L, Williams ZM, et al. Local and distant responses to single pulse electrical stimulation reflect different forms of connectivity. *Neuroimage*. Aug 15 2021;237:118094. doi:10.1016/j.neuroimage.2021.118094
36. Parker CS, Clayden JD, Cardoso MJ, et al. Structural and effective connectivity in focal epilepsy. *NeuroImage: Clinical*. 2018;17:943-952. doi:10.1016/j.nicl.2017.12.020
37. D'Haese P-F, Pallavaram S, Li R, et al. CranialVault and its CRAVE tools: A clinical computer assistance system for deep brain stimulation (DBS) therapy. *Medical Image Analysis*. 2012;16(3):744-753. doi:10.1016/j.media.2010.07.009
38. Engel J. Update on surgical treatment of the epilepsies: Summary of The Second International Palm Desert Conference on the Surgical Treatment of the Epilepsies (1992). 1993;43(8):1612-1612. doi:10.1212/wnl.43.8.1612

39. Revell AY, Silva AB, Arnold TC, et al. A framework For brain atlases: Lessons from seizure dynamics. *Neuroimage*. Jul 1 2022;254:118986. doi:10.1016/j.neuroimage.2022.118986
40. Prime D, Woolfe M, O'Keefe S, Rowlands D, Dionisio S. Quantifying volume conducted potential using stimulation artefact in cortico-cortical evoked potentials. *J Neurosci Methods*. May 1 2020;337:108639. doi:10.1016/j.jneumeth.2020.108639
41. Tournier JD, Smith R, Raffelt D, et al. MRtrix3: A fast, flexible and open software framework for medical image processing and visualisation. *NeuroImage*. 2019;202:116137. doi:10.1016/j.neuroimage.2019.116137
42. Jenkinson M, Beckmann CF, Behrens TEJ, Woolrich MW, Smith SM. FSL. *NeuroImage*. 2012;62(2):782-790. doi:10.1016/j.neuroimage.2011.09.015
43. Tustison NJ, Cook PA, Klein A, et al. Large-scale evaluation of ANTs and FreeSurfer cortical thickness measurements. *NeuroImage*. 2014;99:166-179. doi:10.1016/j.neuroimage.2014.05.044
44. Cai L, Yang Q, Hansen C, et al. PreQual: An automated pipeline for integrated preprocessing and quality assurance of diffusion weighted MRI images. In submission. . 2020;
45. Veraart J, Novikov DS, Christiaens D, Ades-Aron B, Sijbers J, Fieremans E. Denoising of diffusion MRI using random matrix theory. *NeuroImage*. 2016;142:394-406. doi:10.1016/j.neuroimage.2016.08.016
46. Veraart J, Fieremans E, Novikov DS. Diffusion MRI noise mapping using random matrix theory. *Magnetic Resonance in Medicine*. 2016;76(5):1582-1593. doi:10.1002/mrm.26059
47. Cordero-Grande L, Christiaens D, Hutter J, Price AN, Hajnal JV. Complex diffusion-weighted image estimation via matrix recovery under general noise models. *NeuroImage*. 2019;200:391-404. doi:10.1016/j.neuroimage.2019.06.039
48. Schilling KG, Blaber J, Hansen C, et al. Distortion correction of diffusion weighted MRI without reverse phase-encoding scans or field-maps. *PLOS ONE*. 2020;15(7):e0236418. doi:10.1371/journal.pone.0236418
49. Andersson JL, Skare S, Ashburner J. How to correct susceptibility distortions in spin-echo echo-planar images: application to diffusion tensor imaging. *Neuroimage*. Oct 2003;20(2):870-88. doi:10.1016/s1053-8119(03)00336-7
50. Smith SM, Jenkinson M, Woolrich MW, et al. Advances in functional and structural MR image analysis and implementation as FSL. *Neuroimage*. 2004;23 Suppl 1:S208-19. doi:10.1016/j.neuroimage.2004.07.051
51. Andersson JLR, Sotiropoulos SN. An integrated approach to correction for off-resonance effects and subject movement in diffusion MR imaging. *Neuroimage*. Jan 15 2016;125:1063-1078. doi:10.1016/j.neuroimage.2015.10.019
52. Andersson JLR, Graham MS, Zsoldos E, Sotiropoulos SN. Incorporating outlier detection and replacement into a non-parametric framework for movement and distortion correction of diffusion MR images. *Neuroimage*. Nov 1 2016;141:556-572. doi:10.1016/j.neuroimage.2016.06.058
53. Smith RE, Tournier J-D, Calamante F, Connelly A. SIFT2: Enabling dense quantitative assessment of brain white matter connectivity using streamlines tractography. *NeuroImage*. 2015;119:338-351. doi:10.1016/j.neuroimage.2015.06.092
54. Iglesias JE, Cheng-Yi L, Thompson PM, Zhuowen T. Robust Brain Extraction Across Datasets and Comparison With Publicly Available Methods. 2011;30(9):1617-1634. doi:10.1109/tmi.2011.2138152
55. Tustison NJ, Avants BB, Cook PA, et al. N4ITK: Improved N3 Bias Correction. *IEEE Transactions on Medical Imaging*. 2010;29(6):1310-1320. doi:10.1109/tmi.2010.2046908
56. Bhushan C, Haldar JP, Choi S, Joshi AA, Shattuck DW, Leahy RM. Co-registration and distortion correction of diffusion and anatomical images based on inverse contrast normalization. 2015;115:269-280. doi:10.1016/j.neuroimage.2015.03.050

57. Zhang Y, Brady M, Smith S. Segmentation of brain MR images through a hidden Markov random field model and the expectation-maximization algorithm. *IEEE Transactions on Medical Imaging*. 2001;20(1):45-57. doi:10.1109/42.906424
58. Smith SM. Fast robust automated brain extraction. *Human Brain Mapping*. 2002;17(3):143-155. doi:10.1002/hbm.10062
59. Patenaude B, Smith SM, Kennedy DN, Jenkinson M. A Bayesian model of shape and appearance for subcortical brain segmentation. *NeuroImage*. 2011;56(3):907-922. doi:10.1016/j.neuroimage.2011.02.046
60. Tournier JD, Calamante F, Gadian DG, Connelly A. Direct estimation of the fiber orientation density function from diffusion-weighted MRI data using spherical deconvolution. *NeuroImage*. 2004;23(3):1176-1185. doi:10.1016/j.neuroimage.2004.07.037
61. Jeurissen B, Tournier J-D, Dhollander T, Connelly A, Sijbers J. Multi-tissue constrained spherical deconvolution for improved analysis of multi-shell diffusion MRI data. *NeuroImage*. 2014;103:411-426. doi:10.1016/j.neuroimage.2014.07.061
62. Tournier J-D, Calamante F, Connelly A. Improved probabilistic streamlines tractography by 2nd order integration over fibre orientation distributions. *Proceedings of the International Society for Magnetic Resonance in Medicine*. 2009;
63. Smith RE, Tournier J-D, Calamante F, Connelly A. Anatomically-constrained tractography: Improved diffusion MRI streamlines tractography through effective use of anatomical information. *NeuroImage*. 2012;62(3):1924-1938. doi:10.1016/j.neuroimage.2012.06.005
64. Smith RE, Tournier J-D, Calamante F, Connelly A. The effects of SIFT on the reproducibility and biological accuracy of the structural connectome. *NeuroImage*. 2015;104:253-265. doi:10.1016/j.neuroimage.2014.10.004
65. Kajikawa Y, Charles. How Local Is the Local Field Potential? *Neuron*. 2011;72(5):847-858. doi:10.1016/j.neuron.2011.09.029
66. Scharfman HE. The neurobiology of epilepsy. *Current Neurology and Neuroscience Reports*. 2007;7(4):348-354. doi:10.1007/s11910-007-0053-z
67. Naylor DE. Glutamate and GABA in the balance: Convergent pathways sustain seizures during status epilepticus. *Epilepsia*. 2010;51:106-109. doi:10.1111/j.1528-1167.2010.02622.x
68. Shao L-R, Habela CW, Stafstrom CE. Pediatric Epilepsy Mechanisms: Expanding the Paradigm of Excitation/Inhibition Imbalance. *Children*. 2019;6(2):23. doi:10.3390/children6020023
69. Treiman DM. GABAergic Mechanisms in Epilepsy. *Epilepsia*. 2001;42:8-12. doi:10.1046/j.1528-1157.2001.042suppl.3008.x
70. Krook-Magnuson E, Armstrong C, Oijala M, Soltesz I. On-demand optogenetic control of spontaneous seizures in temporal lobe epilepsy. *Nature Communications*. 2013;4(1):1376. doi:10.1038/ncomms2376
71. Ledri M, Madsen MG, Nikitidou L, Kirik D, Kokaia M. Global Optogenetic Activation of Inhibitory Interneurons during Epileptiform Activity. *Journal of Neuroscience*. 2014;34(9):3364-3377. doi:10.1523/jneurosci.2734-13.2014
72. Gunnarsdottir KM, Gonzalez-Martinez J, Wing S, Sarma SV. Sources and Sinks in Interictal iEEG Networks: An iEEG Marker of the Epileptogenic Zone. IEEE;
73. Golnoosh Kamali1, Rachel J. Smith1,2, Mark Hays2, Christopher Coogan4, Nathan E. Crone2,4, Sridevi V. Sarma1,2,3, Member, IEEE, Joon Y. Kang4. Localizing the seizure onset zone from single pulse electrical stimulation responses using transfer function models. 2020;doi:10.1109/EMBC44109.2020.9175954
74. Kundu B, Davis TS, Philip B, et al. A systematic exploration of parameters affecting evoked intracranial potentials in patients with epilepsy. *Brain Stimul*. Jun 3 2020;13(5):1232-1244. doi:10.1016/j.brs.2020.06.002

75. Parker CS, Clayden JD, Cardoso MJ, et al. Structural and effective connectivity in focal epilepsy. *Neuroimage Clin*. 2018;17:943-952. doi:10.1016/j.nicl.2017.12.020
76. Yan Q, Gaspard N, Zaveri HP, et al. The connectivity index: an effective metric for grading epileptogenicity. *Journal of Neurosurgery*. 2019:1-8. doi:10.3171/2019.4.jns195
77. Zhang N, Zhang B, Rajah GB, et al. The effectiveness of cortico-cortical evoked potential in detecting seizure onset zones. *Neurological research*. 2018;40(6):480-490.
78. Jiang H, Kokkinos V, Ye S, et al. Interictal SEEG Resting-State Connectivity Localizes the Seizure Onset Zone and Predicts Seizure Outcome. *Advanced Science*. 2022:2200887. doi:10.1002/advs.202200887
79. Guo Z-h, Zhao B-t, Toprani S, et al. Epileptogenic network of focal epilepsies mapped with cortico-cortical evoked potentials. *Clinical Neurophysiology*. 2020;(131):2657-2666. doi:10.1016/j.clinph.2020.08.012
80. Malladi R, Kalamangalam G, Tandon N, Aazhang B. Identifying Seizure Onset Zone From the Causal Connectivity Inferred Using Directed Information. *IEEE Journal of Selected Topics in Signal Processing*. 2016;10(7):1267-1283. doi:10.1109/jstsp.2016.2601485
81. Itzkovitz S, Alon U. Subgraphs and network motifs in geometric networks. *Physical Review E*. 2005;71(2)doi:10.1103/physreve.71.026117
82. Tempel T, Frings C, Pastötter B. EEG beta power increase indicates inhibition in motor memory. *International Journal of Psychophysiology*. 2020;150:92-99. doi:10.1016/j.ijpsycho.2020.02.008
83. Hammond C, Bergman H, Brown P. Pathological synchronization in Parkinson's disease: networks, models and treatments. *Trends Neurosci*. Jul 2007;30(7):357-64. doi:10.1016/j.tins.2007.05.004
84. Mouthaan BE, Van ‘T Klooster MA, Keizer D, et al. Single Pulse Electrical Stimulation to identify epileptogenic cortex: Clinical information obtained from early evoked responses. 2016;127(2):1088-1098. doi:10.1016/j.clinph.2015.07.031
85. Van 'T Klooster MA, Zijlmans M, Leijten FSS, Ferrier CH, Van Putten MJAM, Huiskamp GJM. Time–frequency analysis of single pulse electrical stimulation to assist delineation of epileptogenic cortex. *Brain*. 2011;134(10):2855-2866. doi:10.1093/brain/awr211
86. Prime D, Woolfe M, Rowlands D, O’Keefe S, Dionisio S. Comparing connectivity metrics in cortico-cortical evoked potentials using synthetic cortical response patterns. *Journal of Neuroscience Methods*. 2020;334:108559. doi:10.1016/j.jneumeth.2019.108559
87. Matsumoto R, Nair DR, LaPresto E, Bingaman W, Shibasaki H, Luders HO. Functional connectivity in human cortical motor system: a cortico-cortical evoked potential study. *Brain*. Jan 2007;130(Pt 1):181-97. doi:10.1093/brain/awl257
88. van Blooijs D, Leijten FSS, van Rijen PC, Meijer HGE, Huiskamp GJM. Evoked directional network characteristics of epileptogenic tissue derived from single pulse electrical stimulation. *Hum Brain Mapp*. Nov 2018;39(11):4611-4622. doi:10.1002/hbm.24309
89. Paulk AC, Zelmann R, Crocker B, et al. Local and distant cortical responses to single pulse intracranial stimulation in the human brain are differentially modulated by specific stimulation parameters. *Brain Stimulation*. 2022;15(2):491-508. doi:10.1016/j.brs.2022.02.017
90. Prime D, Rowlands D, O'Keefe S, Dionisio S. Considerations in performing and analyzing the responses of cortico-cortical evoked potentials in stereo-EEG. *Epilepsia*. Jan 2018;59(1):16-26. doi:10.1111/epi.13939
91. Valentin A. Responses to single pulse electrical stimulation identify epileptogenesis in the human brain in vivo. *Brain*. 2002;125(8):1709-1718. doi:10.1093/brain/awf187
92. Fingelkurts AA, Fingelkurts AA. Short-Term EEG Spectral Pattern as a Single Event in EEG Phenomenology. *The Open Neuroimaging Journal*. 2010;4:130-156. doi:10.2174/1874440001004010130

93. Stein Av, Sarnthein J. Different frequencies for different scales of cortical integration: from local gamma to long range alpha・theta synchronization. *International Journal of Psychophysiology*. 2000;38:301-313.
94. Goyal A, Miller J, Qasim SE, et al. Functionally distinct high and low theta oscillations in the human hippocampus. *Nature Communications*. 2020;11(1)doi:10.1038/s41467-020-15670-6
95. Whittington MA, Traub RD, Kopell N, Ermentrout B, Buhl EH. Inhibition-based rhythms: experimental and mathematical observations on network dynamics. *International Journal of Psychophysiology*. 2000;38(3):315-336. doi:10.1016/s0167-8760(00)00173-2
96. Bartos M, Vida I, Jonas P. Synaptic mechanisms of synchronized gamma oscillations in inhibitory interneuron networks. *Nature Reviews Neuroscience*. 2007;8(1):45-56. doi:10.1038/nrn2044
97. Sohal VS, Zhang F, Yizhar O, Deisseroth K. Parvalbumin neurons and gamma rhythms enhance cortical circuit performance. *Nature*. 2009;459(7247):698-702. doi:10.1038/nature07991
98. Hermes D, Kasteleijn-Nolst Trenité DGA, Winawer J. Gamma oscillations and photosensitive epilepsy. *Current Biology*. 2017;27(9):R336-R338. doi:10.1016/j.cub.2017.03.076
99. Jiruska P, Alvarado-Rojas C, Schevon CA, et al. Update on the mechanisms and roles of high-frequency oscillations in seizures and epileptic disorders. *Epilepsia*. 2017;58(8):1330-1339. doi:10.1111/epi.13830
100. Paredes-Aragon E, AlKhaldi NA, Ballesteros-Herrera D, Mirsattari SM. Stereo-Encephalographic Presurgical Evaluation of Temporal Lobe Epilepsy: An Evolving Science. *Frontiers in Neurology*. 2022;13doi:10.3389/fneur.2022.867458
101. Gotman J. Not Just Where, But How Does a Seizure Start? *Epilepsy Currents*. 2019;19(4):229-230. doi:10.1177/1535759719854756
102. Lundstrom BN, Gompel JV, Khadjevand F, Worrell G, Stead M. Chronic subthreshold cortical stimulation and stimulation-related EEG biomarkers for focal epilepsy. *Brain Communications*. 2019;1(1)doi:10.1093/braincomms/fcz010
103. Zamani Esfahlani F, Faskowitz J, Slack J, Mišić B, Betzel RF. Local structure-function relationships in human brain networks across the lifespan. *Nature Communications*. 2022;13(1)doi:10.1038/s41467-022-29770-y
104. Shah P, Ashourvan A, Mikhail F, et al. Characterizing the role of the structural connectome in seizure dynamics. *Brain*. 2019;142(7):1955-1972. doi:10.1093/brain/awz125
105. Myers JC, Smith EH, Leszczynski M, et al. The Spatial Reach of Neuronal Coherence and Spike-field Coupling across the Human Neocortex. *The Journal of Neuroscience*. 2022:JN-RM-0050-22. doi:10.1523/JNEUROSCI.0050-22.2022
106. Betzel RF, Bassett DS. Specificity and robustness of long-distance connections in weighted, interareal connectomes. *Proceedings of the National Academy of Sciences*. 2018;115(21):E4880-E4889. doi:10.1073/pnas.1720186115
107. Thivard L, Adam C, Hasboun D, et al. Interictal diffusion MRI in partial epilepsies explored with intracerebral electrodes. *Brain*. 2006;129(2):375-385. doi:10.1093/brain/awh709
108. Besson P, Bandt SK, Proix T, et al. Anatomic consistencies across epilepsies: a stereotactic-EEG informed high-resolution structural connectivity study. *Brain*. Oct 1 2017;140(10):2639-2652. doi:10.1093/brain/awx181
109. Donos C, Maliia MD, Mindruta I, et al. A connectomics approach combining structural and effective connectivity assessed by intracranial electrical stimulation. *Neuroimage*. May 15 2016;132:344-358. doi:10.1016/j.neuroimage.2016.02.054
110. Kini LG, Bernabei JM, Mikhail F, et al. Virtual resection predicts surgical outcome for drug-resistant epilepsy. *Brain*. 2019;142(12):3892-3905. doi:10.1093/brain/awz303

111. Olmi S, Petkoski S, Guye M, Bartolomei F, Jirsa V. Controlling seizure propagation in large-scale brain networks. *PLoS Comput Biol*. Feb 2019;15(2):e1006805. doi:10.1371/journal.pcbi.1006805
112. Proix T, Bartolomei F, Guye M, Jirsa VK. Individual brain structure and modelling predict seizure propagation. *Brain*. 2017;140(3):641-654. doi:10.1093/brain/awx004
113. Gleichgerrcht E, Greenblatt AS, Kellermann TS, et al. Patterns of seizure spread in temporal lobe epilepsy are associated with distinct white matter tracts. *Epilepsy Research*. 2021;171:106571. doi:10.1016/j.eplepsyres.2021.106571
114. Baum GL, Cui Z, Roalf DR, et al. Development of structure-function coupling in human brain networks during youth. *Proc Natl Acad Sci U S A*. Jan 7 2020;117(1):771-778. doi:10.1073/pnas.1912034117
115. Conrad EC, Bernabei JM, Kini LG, et al. How sensitive is functional connectivity to electrode resampling on intracranial EEG? Implications for personalized network models in drug-resistant epilepsy. Cold Spring Harbor Laboratory; 2019.
116. Conrad EC, Bernabei JM, Kini LG, et al. The sensitivity of network statistics to incomplete electrode sampling on intracranial EEG. *Network Neuroscience*. 2020:1-52. doi:10.1162/netn_a_00131
117. Andrews JP, Gummadavelli A, Farooque P, et al. Association of Seizure Spread With Surgical Failure in Epilepsy. *JAMA Neurology*. 2019;76(4):462. doi:10.1001/jamaneurol.2018.4316

Tables

Table 1: Subject characteristics

	Full Cohort (n=81)	**SPES Sub-Cohort (n=23)**	**Diffusion Sub-Cohort (n=26)**
Sex, female (count, percent)	46 (56.8%)	16 (69.6%)	20 (76.9%)
Age (years, mean ± STD)	34.4 ± 12.1	36.7 ± 11.7	35.2 ± 11.5
Epilepsy duration (years, mean ± STD)	16.4 ± 11.9	15.1 ± 9.0	14.8 ± 10.6
FBTC seizures, yes (count, percent)	58 (71.6%)	18 (78.2%)	17 (65.4%)
MTS, yes (count, percent)	15 (18.5%)	3 (13.0%)	6 (23.1%)
Surgery type			
Resective SAH	14 (17.3%)	3 (13.0%)	8 (30.8%)
TL	11 (13.6%)	3 (13.0%)	3 (11.5%)
Other resection	10 (12.3%)	1 (4.3%)	2 (7.7%)
Laser SAH	4 (4.9%)	0 (0%)	0 (0%)
RNS	24 (29.6%)	10 (43.5%)	11 (42.3%)
DBS	1 (1.2%)	0 (0%)	0 (0%)
None	17 (21.0%)	6 (26.1%)	2 (7.7%)
Follow-up duration* (months, mean ± STD)	26.7 ± 17.6	12.8 ± 7.8	35.3 ± 19.0
SEEG Nodes Analyzed (mean ± STD)	85.4 ± 26.7	93.3 ± 19.0	78.8 ± 23.9
SEEG Nodes Stimulated (mean ± STD)	NA	60.0 ± 10.7	NA

DBS = deep brain stimulation of bilateral anterior thalamic nuclei; FBTC = focal to bilateral tonic-clonic seizures; MTS = mesial temporal sclerosis; RNS = responsive neurostimulation; SAH = selective amygdalohippocampectomy; SEEG = stereo-electroencephalography; SPES = single-pulse electrical stimulation; STD = standard deviation; TL = temporal lobectomy; * Only for resective surgeries.

Figures

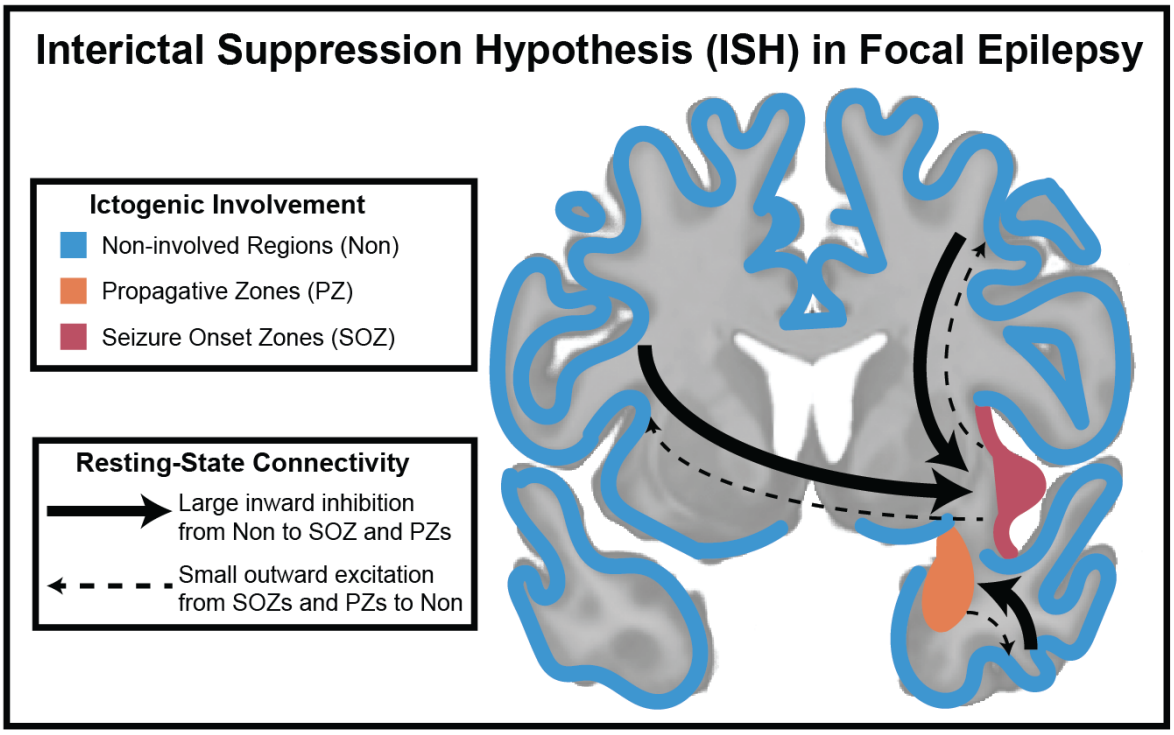

Figure 1: Interictal Suppression Hypothesis (ISH) in focal epilepsy. The ISH proposes that regions not involved in ictogenesis (Non, blue) have an active role in suppressing seizure onset zones (SOZ, red) and propagative zones (PZ, orange) through brain network interactions that can be observed electrographically.

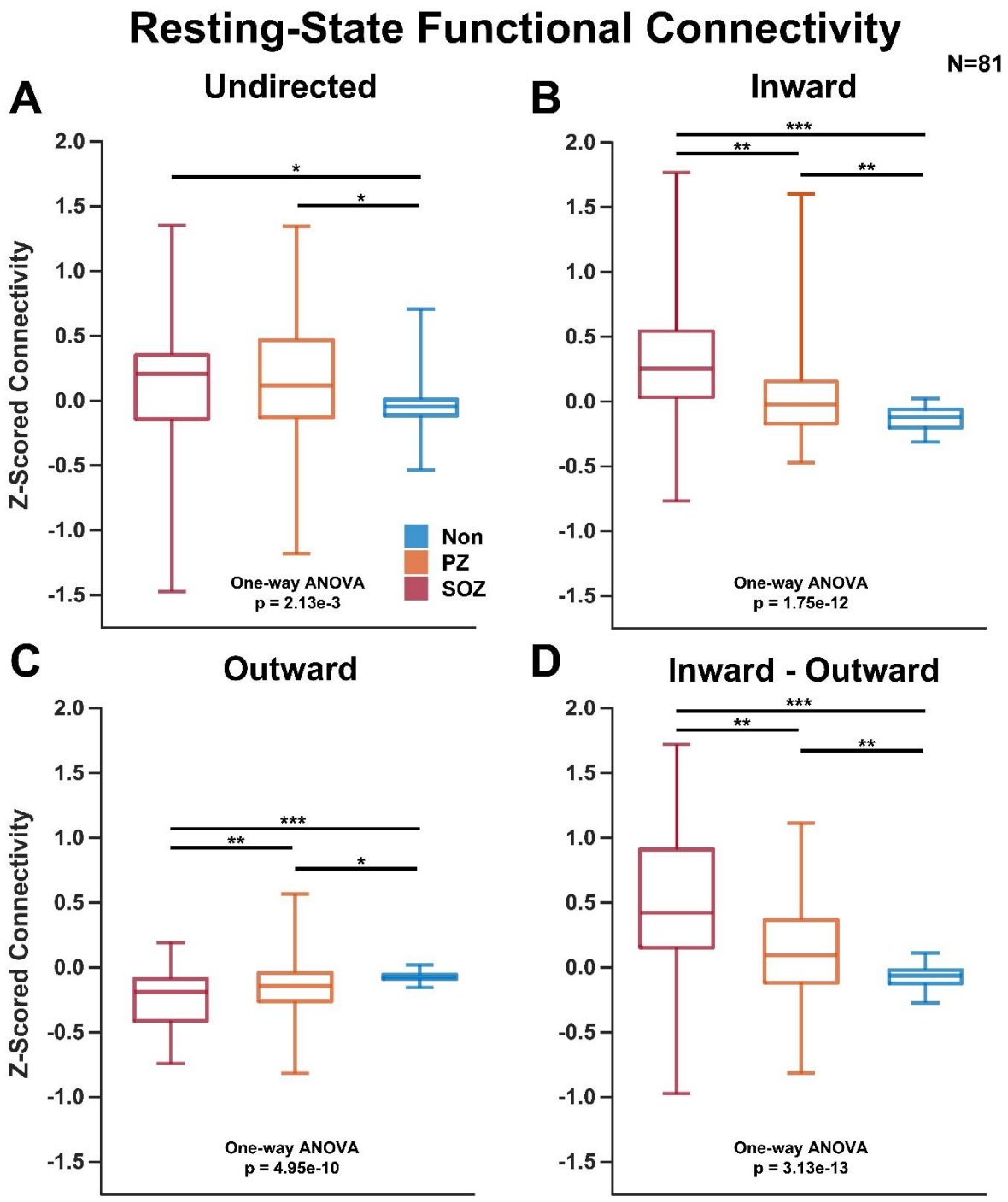

Figure 2: Resting-state SEEG connectivity. A) Undirected alpha-band imaginary coherence was elevated for SOZs and PZs (one-way ANOVA p-value=2.13e-3 with post-hoc multiple pairwise t-test comparisons significant for SOZ-Non and PZ-Non. **B)** Inward partial directed coherence strength was elevated significantly for SOZs and PZs (one-way ANOVA p-value=1.75e-12 with post-hoc multiple pairwise t-test comparisons significant between all three groups. **C)** Outward partial directed coherence strength was significantly lower for SOZs and PZs (one-way ANOVA p-value=4.95e-10 with post-hoc multiple pairwise t-test comparisons significant between all three groups. **D)** Inward – outward (reciprocal) connectivity exhibited a stronger signal to that of inward or outward separately (one-way ANOVA p-value=3.13-13 with post-hoc multiple pairwise t-test comparisons significant between all three groups). Box represents first quartile, mean, and third quartile. Whiskers represent maximum and minimum. *p<5e-2, **p < 5e-3, ***p< 5e-6. N=81 subjects.

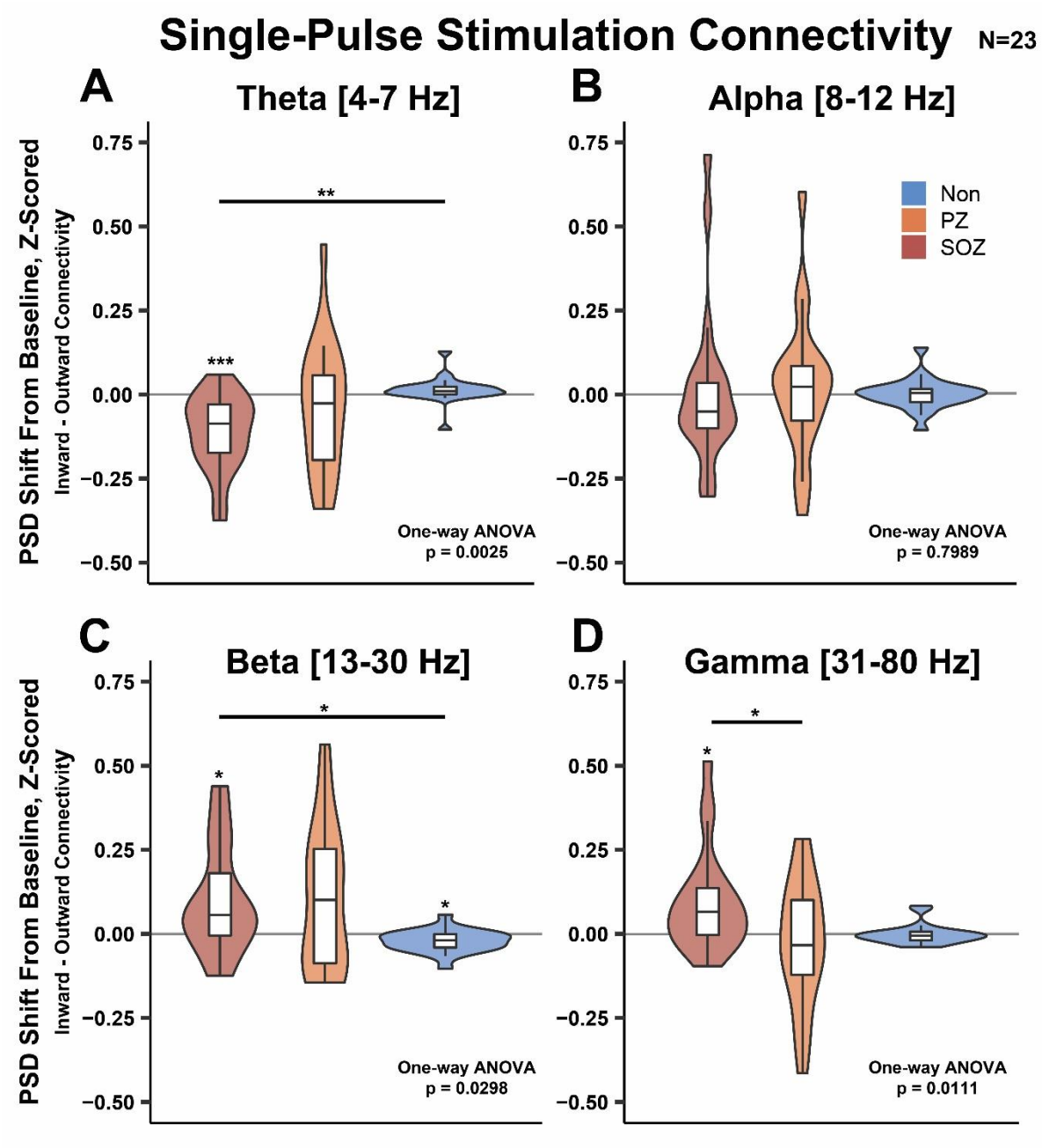

Figure 3: SPES connectivity. Frequency-band specific low-frequency stimulation induced change in power spectral density from pre-stimulation baseline. **A)** SOZ theta power is reduced when non-SOZ SEEG contacts are stimulated. **B)** Alpha band power was not observed to be significantly altered during stimulation. **C-D)** Beta and gamma band power in SOZs were elevated when non-SOZs were stimulated. *p<5e-2, **p < 5e-3, ***p< 5e-6. N=23 subjects.

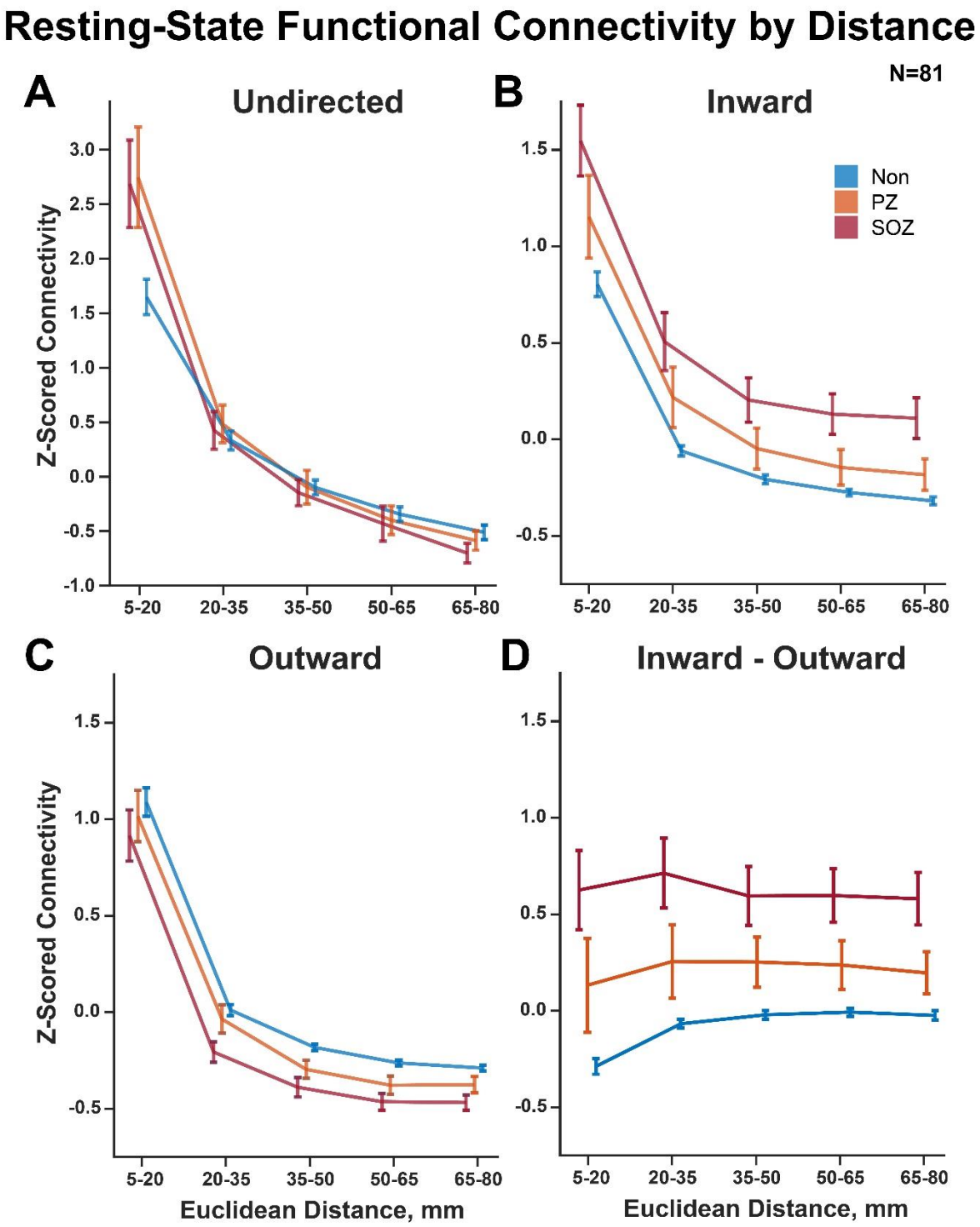

Figure 4: SEEG resting-state connectivity over Euclidean distance. A-C) Undirected and directed connectivity declined rapidly with increasing network edge Euclidean distance thresholds (two-way repeated measures ANOVA distance effect p-value<1e-10 for undirected inward and outward connectivity). **D)** Reciprocal connectivity (inward – outward PDC strength) demonstrates a consistent relationship spanning all distance thresholds measured (two-way repeated measures ANOVA group effect p-value=2.6e-12, interaction p-value=1.15e-6). Error bars represent 95% confidence intervals of the mean.

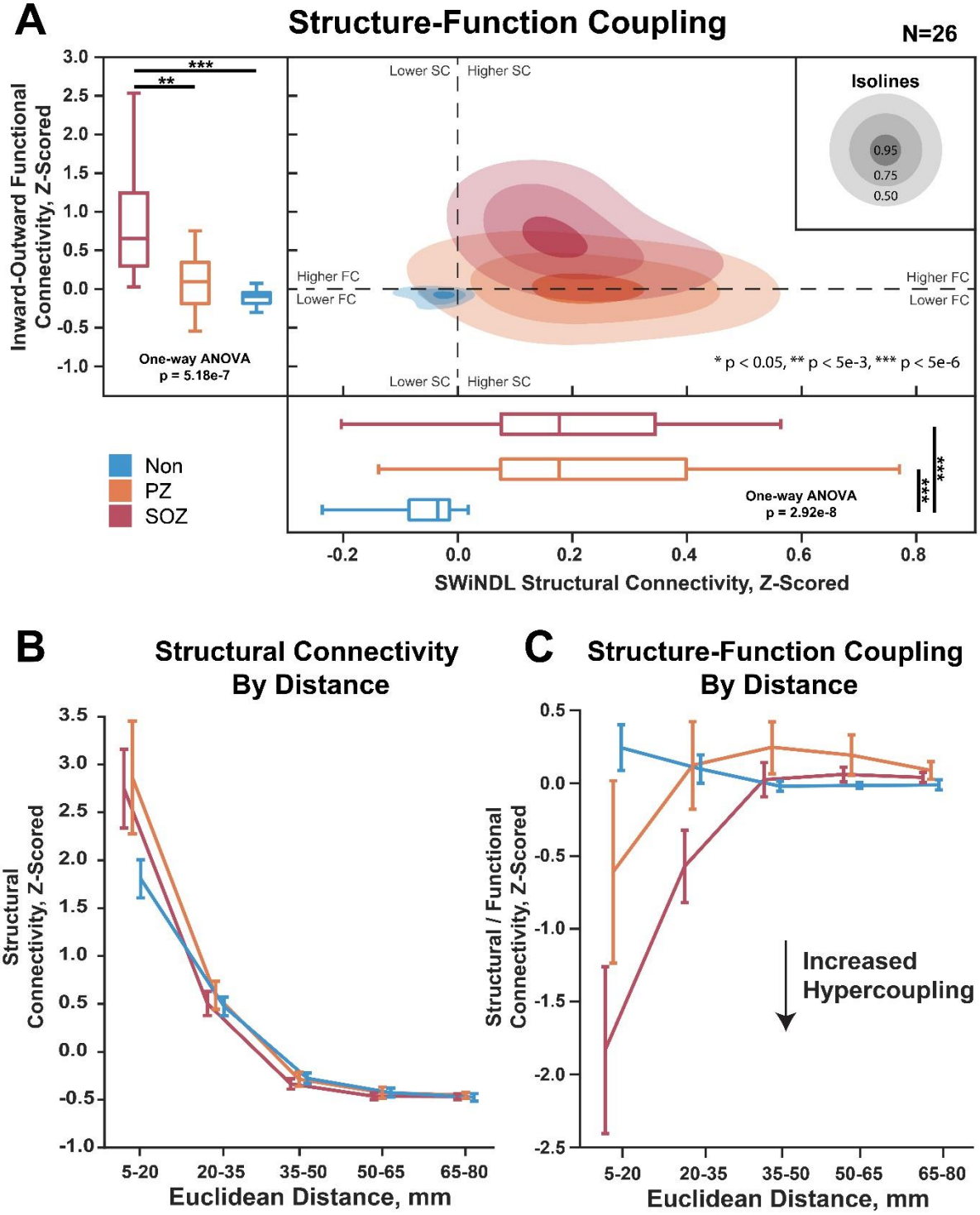

Figure 5: Structure-function coupling over Euclidean distance. A) The left boxplots show the functional connectivity (partial directed coherence inward strength minus outward strength) of seizure onset zones (SOZ), propagative zones (PZ), and non-involved regions (Non). The bottom boxplots show structural connectivity as measured by SWiNDL (Subsampling Whole-brain tractography with intracranial EEG Near-field Dynamic Localization). The contours in the middle show the 2D distribution of the scatterplot of functional vs. structural connectivity. B) Structural connectivity over Euclidean edge distance. Error bars represent 95% confidence intervals. Repeated measures two-way ANOVA: SOZ/PZ/Non effect p=7.52e-3, distance effect p=1.75e-64, interaction effect p=5.44e-9. C) Structural/Functional connectivity over Euclidean edge distance. Repeated measures two-way ANOVA: SOZ/PZ/Non effect p=7.27e-4, distance effect p=8.63e-19, interaction effect p=9.76e-21. Post-ANOVA multiple comparison: **p < 5e-3, ***p< 5e-6. N=26 patients.

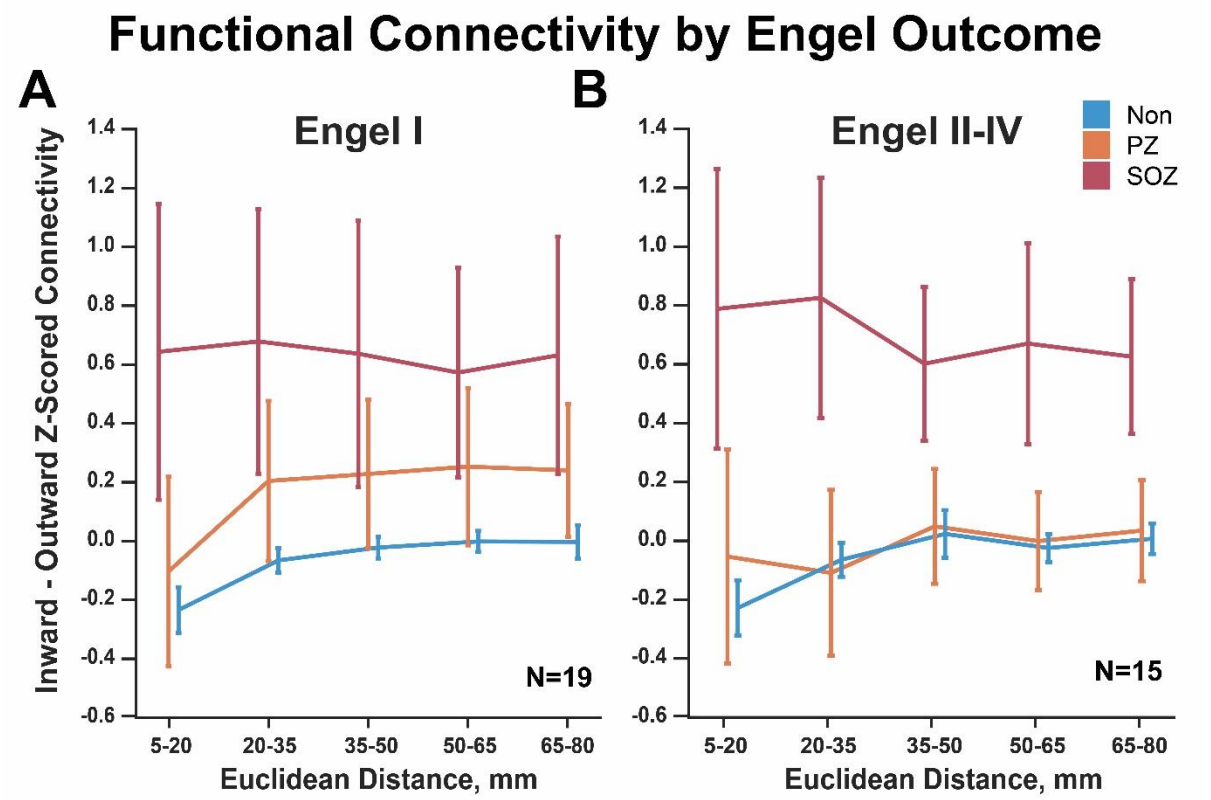

Figure 6: Functional connectivity by Engel outcome. A) SOZ, PZ, and non-involved region connectivity for subjects with Engel 1 outcomes (two-way repeated measures ANOVA group effect p-value = 1.16e-2, distance effect -value=1.26e-2, interaction p-value=5.15e-2). **B)** PZs exhibit lower connectivity in subjects with Engel II-IV outcomes (two-way repeated measures ANOVA group effect p-value=1.73e-4, distance effect p-value=7.83e-1, interaction p-value=3.01e-3). Error bars represent 95% confidence intervals of the mean.

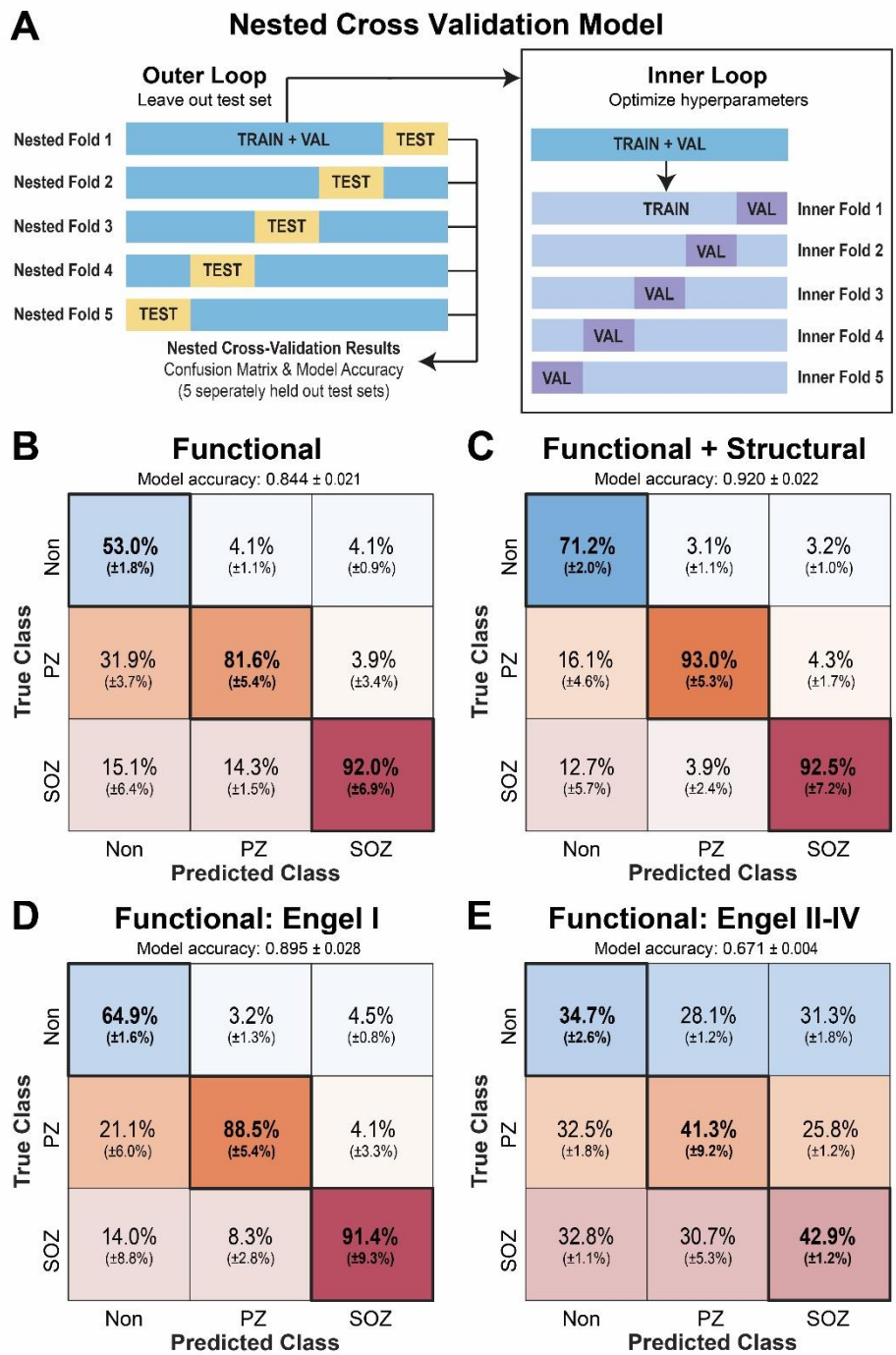

Figure 7: Classification of SOZ, PZ, and non-involved regions using a support vector machine. A) A 5-fold nested cross validation scheme was used to evaluate the support vector machine's ability to classify SOZ vs. PZ vs Non. A completely withheld testing set delineated at the patient level was used for each model evaluation. **B)** Confusion matrix when only functional connectivity was used to generate the model. Overall held-out test set accuracy of 84.4±2.1% (mean ± STD). Confusion matrix percentages are normalized by column – i.e., each confusion matrix entry can be interpreted as "If the model predicts this SEEG contact is a [SOZ/PZ/Non], then there is an X% chance it truly is." **C)** Confusion matrix for a model using functional and structural connectivity with overall held-out test set accuracy of 0.920±2.2%. **D)** Confusion matrix for a model generated with only Engel I subjects with overall held-out test set accuracy of 89.5±2.8% **E)** Confusion matrix for Engel II-IV subjects tested with the model generated from Engel I subjects (i.e. model "D") with overall held-out test set accuracy of 67.1±0.4%.